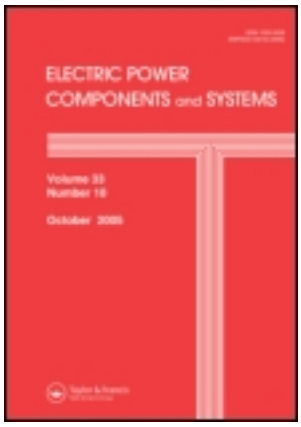

Electric Power Components and Systems
Publication details, including instructions for authors and subscription information:
http://www.tandfonline.com/loi/uemp20

Detection of Winding Radial Deformation in Power Transformers by Confocal Microwave Imaging

Raziyeh Mosayebi[a], Hamid Sheikhzadeh[a], Mohammad Sadegh Golsorkhi[a], Maryam Sadat Akhavan Hejazi[b] & Gevorg B. Gharehpetian[a]
[a] Electrical Engineering Department, Amirkabir University of Technology, Tehran, Iran
[b] [b]Electrical Engineering Department, University of Kashan, Kashan, Iran
Published online: 13 Mar 2014.

To cite this article: Raziyeh Mosayebi, Hamid Sheikhzadeh, Mohammad Sadegh Golsorkhi, Maryam Sadat Akhavan Hejazi & Gevorg B. Gharehpetian (2014) Detection of Winding Radial Deformation in Power Transformers by Confocal Microwave Imaging, Electric Power Components and Systems, 42:6, 605-611, DOI: 10.1080/15325008.2014.880964

To link to this article: http://dx.doi.org/10.1080/15325008.2014.880964

Electric Power Components and Systems, 42(6):605–611, 2014

ISSN: 1532-5008 print / 1532-5016 online
DOI: 10.1080/15325008.2014.880964

Taylor & Francis
Taylor & Francis Group

Detection of Winding Radial Deformation in Power Transformers by Confocal Microwave Imaging

Raziyeh Mosayebi,[1] Hamid Sheikhzadeh,[1] Mohammad Sadegh Golsorkhi,[1] Maryam Sadat Akhavan Hejazi,[2] and Gevorg B. Gharehpetian[1]
[1]Electrical Engineering Department, Amirkabir University of Technology, Tehran, Iran
[2]Electrical Engineering Department, University of Kashan, Kashan, Iran

CONTENTS

Abstract—In this article, a new bi-static method for the detection and determination of magnitude and location of winding radial deformation in power transformers has been proposed. In this method, which is based on confocal microwave imaging, a ultra-wideband transceiver is utilized to emit a short pulse toward the transformer winding and determine its reflection at several points along a linear path. The measured signals are then processed to obtain a 2D image of the winding. The effectiveness of this algorithm for radial deformation is demonstrated through four different experiments. The resultant image provides satisfactory information of the magnitude and position of the radial deformation in transformer.

1. INTRODUCTION

Power transformers are fundamental and valuable parts of electric power systems. Therefore, their careful monitoring [1] and fault assessment is of high importance. The winding mechanical faults that are caused by the mechanical forces incurred during short circuit or transportation might occur in radial direction (radial deformation) or axial direction (axial displacement). Radial deformation consists of a protuberance on the surface of the transformer winding, while the axial displacement in its simplest form shifts the winding in the upward or downward direction.

Several methods to detect winding mechanical faults have been presented in the literature. For example, the scattering parameter method has been used for the diagnosis of winding displacements [2–4]. In [4], scattering parameters were obtained and their magnitudes and phases stored in a database for the classification. The *k*-nearest neighbor (KNN) and decision tree classifiers are then employed, and the superiority of the KNN over the decision tree classifier is shown. The other common approach for transformer fault detection is the transfer function method [5–7]. For instance, in [7], transfer functions were calculated for the detection of the anomaly in transformer windings, and the

Keywords: microwave imaging, power transformers, fault diagnosis, fault location, transformer winding, radial deformation
Received 9 June 2013; accepted 4 January 2014
Address correspondence to Miss Raziyeh Mosayebi, Electrical Engineering Department, Amirkabir University of Technology, No. 424, Hafez Ave., Tehran, Iran, 15875-4413. E-mail: r_mosayebi@aut.ac.ir
Color versions of one or more of the figures in the article can be found online at www.tandfonline.com/uemp.

lack of transparency was improved by a vector space-based perspective. In [8], variations of the transformer characteristic impedance were used as a signature to detect different defects in the windings. Many other methods have been employed to detect the transformer winding faults, such as the low-voltage impulse and short-circuit impedance methods [9]. Also, the more recent ultra-wide band (UWB) sensor method has been used for the monitoring of the transformer winding [10–12].

In this article, a novel beam-forming method for the detection of radial deformation is presented. It is based on confocal microwave imaging (CMI), which has been utilized for early detection of breast cancer [13–15]. This method is widely used to detect tumors in breast tissue. The physical basis for microwave imaging used in tumor detection lies in the significant contrast in the dielectric properties between the normal breast tissue and the malignant tissue at microwave frequencies. Therefore, a tumor behaves as a scatterer and reflects the incident pulse more strongly compared to other parts of the tissue. This basic concept is used to detect the deformation in transformer windings. Various deformations in transformer windings cause different shapes in the transformer, so the received signals before and after deformation cause different diffractions and scattering strengths. Consequently, this method is able to detect deformation in the resulting 2D images. The proposed method can detect major types of mechanical faults while the transformer is in service (on-line).

To gain more information about the winding, the transceiver antenna is moved in a linear path, and the process of transmitting and receiving is repeated at a number of points. In each location, UWB pulses are transmitted from the antenna, the backscattered responses from the transformer windings are received by the receiver, and the backscattered energy distribution is coherently calculated. Then by utilizing the UWB CMI method, an image of the winding is reconstructed. In the resultant image, the winding appears as a circle. If radial deformation occurs, it appears as a protuberance in the resultant image. Therefore, one can detect the radial deformation by examining the UWB image of the winding. In addition, since the position of the protuberance in the image matches that on the winding, the position of the radial deformation can be detected, as well.

The proposed method is verified by conducting a number of tests on a transformer model. A radial deformation is created on different positions of the model, and the CMI method is implemented to form an image of the model for each case. The resultant images demonstrate the effectiveness of the proposed method for the detection as well as determination of the position of the radial deformation.

This article is organized as follows. In Section 2, the UWB radar imaging is described. In Section 3, the CMI algorithm for image formation is presented, and in Section 4, four different experiments are provided to illustrate the effectiveness of the algorithm. Finally, in Section 5, the article is concluded.

2. UWB RADAR IMAGING

In UWB imaging, there are generally three different ways to obtain signals from a target: mono-static [16], bi-static [17], and multi-static [18, 19]. This study employs the bi-static approach, which is a better fit to the setup and configuration.

Figure 1 depicts the data-measuring process. A transceiver is used to generate a short pulse and propagate it through the antenna. The propagated wave hits the target and provides some information about the impulse response of the target.

Using a broad-beam antenna [20], the target can be "seen" from a wide range of points on the X-axis. By sliding the antenna on the X-axis, more information from the target is collected. The process of measuring the response is repeated at predefined measuring points along the X-axis.

The distance between adjacent measuring points (measuring point step-size) is constant for the process of data registration. To increase the resolution of the image, the measuring point range should be chosen to be as wide as possible.

The reflected response, measured at a point, is called a scan. The set of all scans forms a 2D signal, which is a function of both time and measuring position. It is further processed to form a 2D image of the target [21].

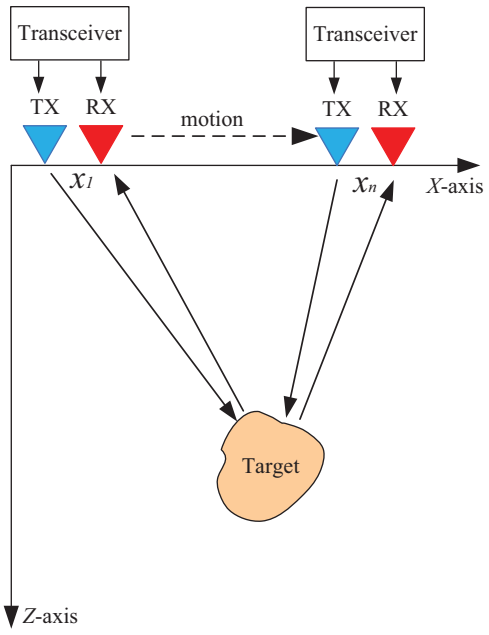

FIGURE 1. Data measuring process using UWB radar imaging.

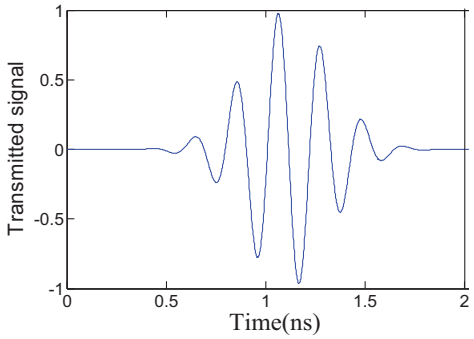

FIGURE 2. Transmitted UWB pulse.

The UWB imaging can be conducted using different kinds of pulses and modulations. In this article, a Gaussian pulse modulated by a sinusoidal carrier is utilized. Figure 2 depicts the UWB pulse.

Before employing the CMI method, the received signals should be preprocessed to remove backscattered signals that are not originating from the transformer and to compensate the propagation loss of the signal amplitude [11].

The received signal at the antenna contains the direct line-of-sight signal, the response from the transformer plus noise, and the interference signals resulting from multi-path reflection, which are received later than the transformer reflection.

Figure 3 depicts a sample scan. It consists of three parts. The first part is the incident pulse received in the receiver, called cross-talk. The second part is the target reflection, which is the desired signal. The third part, which consists of reflections from such objects as walls and desks, is called ambient.

Before removing the cross-talk and ambient sections, the time zero of the scan, *i.e.*, the instant of the transmission of the UWB pulse, must be estimated. Therefore, first of all, the time delay of cross-talk signal (T_{TXRX}) is calculated as the distance between *TX* and *RX* divided by wave speed. If the cross-talk

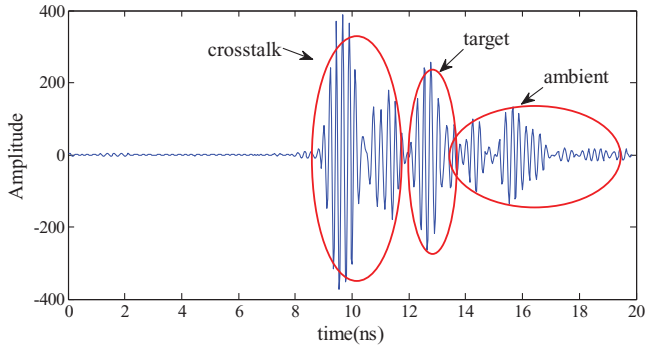

FIGURE 3. Different parts of a sample scan.

signal peaks at τ_{ct}, the time zero (τ_0) is calculated as follows:

$$\tau_0 = \tau_{ct} - T_{TXRX}. \tag{1}$$

As it can be seen in Figure 3, since the transformer is far enough from the two antennas, the desired part of the received signal, which is the transformer reflection, is separable. Therefore, a time windowing approach can be employed to remove the undesired signals.

This rectangular window is given by

$$w(n) = \begin{cases} 1, & T_{Pulse} < n < T_{Pulse} + N \\ 0, & otherwise \end{cases}, \tag{2}$$

where T_{Pulse} is the duration of the transmitted pulse, and N is the window length. The window length is chosen so that the ambient signal can be eliminated. After eliminating the undesired content of the received signal, for coherent processing, the windowed signals are delayed by a number of samples and aligned with the return from the desired focal point (the point at location r_0). This time delay can be computed by the transmitter and receiver locations and the location of focal point, as follows:

$$n_i(r_0) = \frac{1}{\Delta t}\left\lfloor \frac{\|r_{iT} - r_0\|}{c} + \frac{\|r_{iR} - r_0\|}{c} \right\rfloor. \tag{3}$$

Finally, the effect of the propagation attenuation is considered. Since the target is metallic and the reflection is strong enough, there is not much attenuation; therefore, the signal amplitudes are normalized to their maximum for image formation.

3. CMI ALGORITHM

Delay and sum (DAS) beam-forming is a CMI algorithm that has been widely used in medical applications [14, 15, 17]. The first step in the algorithm is preprocessing. During the focusing, the focal point changes from one place to another in the imaging plane, forming various spatial beams [22–24].

At each location, all values of time-shifted signals are squared and coherently added up. Then integration is performed on the summation, and therefore [13],

$$I(\vec{r}_0) = \int_0^L \sum_i^M [y_i(n_i(\vec{r}_0))]^2, \tag{4}$$

where $I(\vec{r}_0)$ is the intensity of the focal point $\vec{r}_0$, $y(\vec{r}_0)$ is the pre-processed signal at the receiver, and $n_i(r_0)$ is the time delay computed for alignment. The index i represents the ith measuring point, and M is the number of measuring points as described in Section 2. L, the time interval of the integration, is based on the application bandwidth, *i.e.*, the bandwidth of the incident pulse that is used in the setup.

To preserve image details at various points of the object, the square in Eq. (5) is eliminated, as follows:

$$I(\vec{r}_0) = \int_0^L \sum_i^M y_i(n_i(\vec{r}_0)). \quad (5)$$

When the transformer responses in windowed received signals are coherent, most of the samples of $I(\overrightarrow{r_0})$ must be positive. The more incoherent the responses are, the more samples will be negative in $I(\overrightarrow{r_0})$. Therefore, as r_0 approaches the transformer location, these aligned signals will become more coherent, and larger positive values will be produced in $I(\overrightarrow{r_0})$. In contrast, for points far from the transformer location, Eq. (5) gets greater negative values. Therefore, these negative values are disregarded (replaced with zeros), and the resultant matrix $I(\overrightarrow{r_0})$ is shown as a 2D RGB image [24].

This algorithm can be summarized as follows.

Step 1. The time zero for all received signals is determined.
Step 2. A time window with appropriate length is designed and applied to separate the target from received signals.
Step 3. The signals are time aligned with respect to each focal point for coherent processing.
Step 4. The windowed and time-aligned signals $y(r_0)$. are calibrated for loss compensation.
Step 5. The summation of the signals in Step 4 is integrated to compute the intensity for each focal point.
Step 6. The negative values of the resultant matrix are replaced with zeros, and then the matrix $I(\overrightarrow{r_0})$ is depicted as an RGB image.

4. EXPERIMENTAL RESULTS

In this article, to implement the UWB imaging process, the setup and winding model in [12] are used. This winding is shown in Figure 4.

Figure 5 shows the top view of the experiments. The model is shown as a circle with a rectangular protuberance on its surface, representing the radial deformation. The antennas movement direction and the wave propagation direction are marked as the X- and Z-axis, respectively. The dimensions of the radial deformation are indicated as R_{dif} and D_{dif}. The resulted DAS image is expected to resemble Figure 5. Note that the antennas are located at the left side of the model. Therefore, most of the incident waves hit the left section, and consequently, most of the reflected waves originate from it. As a result, this section of the model is highlighted in the resultant image.

To assess the performance of the proposed method, a scenario with four different experiments is implemented. In the first experiment, the winding is intact, with no radial deformation. With respect to the observer in the Figure 5, in the second, third, and fourth experiments, a radial deformation of a certain size is created in the right, left, and center of the transformer disks, respectively.

FIGURE 4. Winding model used for testing the algorithm.

These four experiments resemble radial deformations with different positions in a real transformer winding. The specifications of the experiment on the model are given in [12]. The measuring step, the distance between adjacent measuring points, is selected to be smaller than half of the wavelength of the UWB center frequency (31 mm in this article). The number of measuring points is determined based on the measuring span (1200 mm in the setup). The size of the radial deformation is $D_{dif} = 40$ cm and $R_{dif} = 20$ cm.

To each experiment, the CMI method is applied. This includes measuring the scans, preprocessing, and beam-forming steps. L, the appropriate length of integration step, is ten samples of the aligned signals, which is adjusted experimentally. Then the 2D image function ($I(\overrightarrow{r_0})$) is plotted in a color-map scale to get a 2D image of the model. In color-map scale plots,

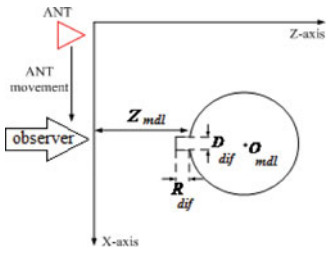

FIGURE 5. CMI experiment: (a) experimental setup (1, receiver; 2, transmitter; 3, transmitting antenna; 4, receiving antenna; 5, transformer winding model) and (b) top view of experimental setup.

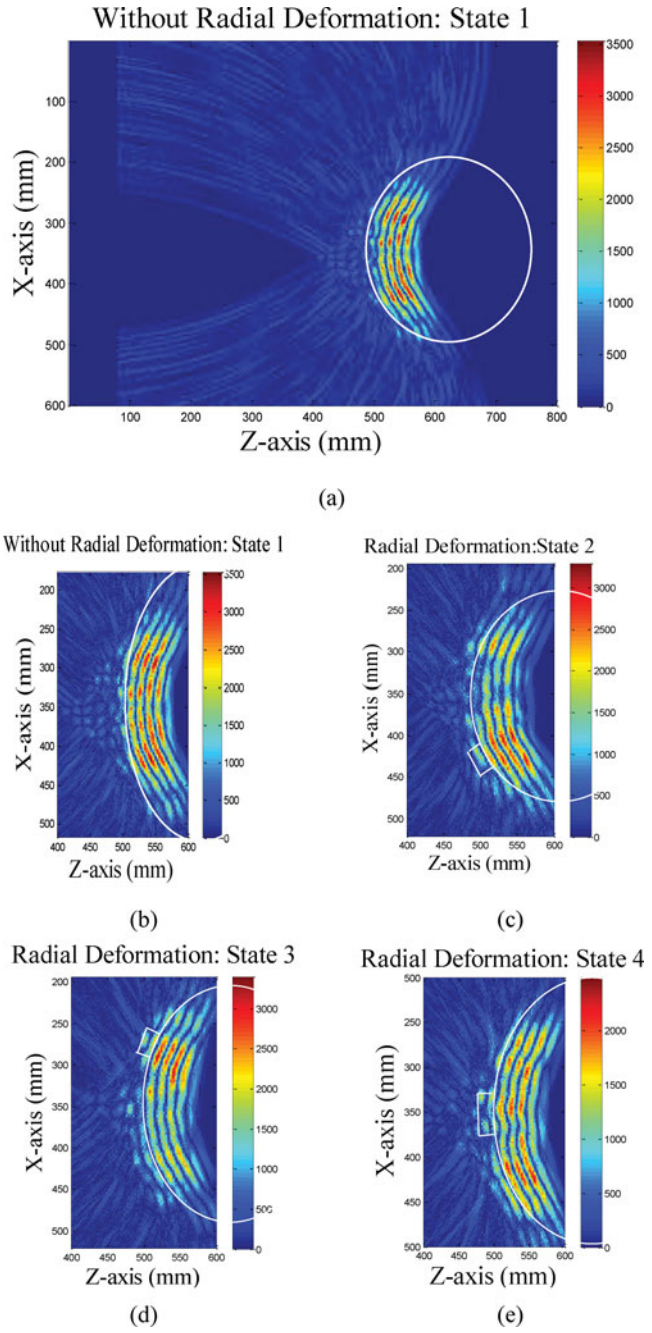

FIGURE 6. DAS images of the model: (a) experiment 1, (b) magnified version of experiment 1, (c) experiment 2, (d) experiment 3, and (e) experiment 4.

the color of a pixel indicates the magnitude of the image function at that pixel. Cold colors imply a low magnitude, while warm colors depict a higher value.

Figure 6(a) depicts the resultant image of the model, without radial deformation (experiment 1). In this image and subsequent DAS image, the model appears as a number of red arcs. The multiple arcs are caused by the form of the UWB pulse. Each period of the sinusoid carrier could produce a peak in the image function, resulting in more than one peak caused by only one surface reflection. In Figure 6(b), the DAS image is magnified for enhanced observation. As shown in this figure, the arcs have a rather uniform pattern, without an asymmetric hot spot. This form of arcs indicates an intact winding with no radial deformation.

Figures 6(c)–6(e) illustrate the DAS images of the model with the deformation on the right, left, and center of the windings with respect to the observer in Figure 6, respectively. In the first case, Figure 6(c), the hot spots are at the right side of transformer due to fragment displacement. In Figure 6(d), the displacement is represented as a hot spot at the left side, and in Figure 6(e), the fragment displacement results in a deformation in arc shapes at the centers of arcs. The legend at the right side of the image depicts the magnitude associated with each color of the color spectrum.

In each figure, the correct place of the deformation is marked by a white rectangular shape. It can be seen in the figures that the beam-forming algorithm is able to detect and determine the location of radial deformation modeled by fragment displacement in the transformer winding.

Comparing the results with those of [12], both algorithms are with high resolution and high information about the size and position of the fragment. The images are clear, and the winding deformation can be detected with a comparison of the images obtained before and after fragment displacement. Although CMI shows clear and comparable results, it takes more time for the algorithm to obtain the final image. On the other hand, the Kirchhoff algorithm is fast and needs less time to get the final result. However, regarding the implementation, CMI has simpler mathematics and is straightforward.

Considering the industrial requirements, the fast running time of the Kirchhoff method makes it more convincing to be used as an algorithm for fault-detection applications.

5. CONCLUSION

A new method based on the CMI approach has been presented to detect and localize the radial deformation of the transformer winding. Using this method, it is possible to obtain a 2D image of the winding. To verify the effectiveness of the proposed method, a test setup, including a transformer winding model and a UWB transceiver, has been employed. The experimental test results show that by using 2D images of transformer model, it is possible to detect the occurrence of the radial deformation, its dimension, and its position. Compared with the Kirchhoff method, CMI is simpler but suffers from a long running time. Both methods, however, show satisfactory results about the size and position of the fragment.

REFERENCES

[1] Naderi, M. S., Blackburn, T. R., Phung, B. T., Naderi, M. S., Ghaemmaghami, R., and Nasiri, A., "Determination of partial discharge propagation and location in transformer windings using a hybrid transformer model," *Elect. Power Compon. Syst.*, Vol. 35, No. 6, pp. 607–623, 2007.

[2] Hejazi, M. A., Gharehpetian, G. B., Moradi, G., Alehosseini, H. A., and Mohammad, M., "On-line monitoring of transformer winding axial displacement and its extent using scattering parameters and k-nearest neighbor method," *IET Generat. Transm. Distribut.*, Vol. 5, No. 8, pp. 824–832, October 2011.

[3] Mokhtari, G., Gharehpetian, G. B., Faraji-dana, R., and Hejazi, M. A., "On-line monitoring of transformer winding axial displacement using UWB sensors and neural network," *Int. Rev. Elect. Eng. (IREE)*, Vol. 5, No. 5, pp. 2122–2128, October 2010.

[4] Hejazi, M. A., Gharehpetian, G. B., Moradi, G. R., Mohammadi, M., and Alehoseini, H. A., "Application of classifiers for on-line monitioring of transformer winding axial displacement by electromagnetic non-destructive testing," *Elect. Power Compon. Syst.*, Vol. 39, No. 4, pp. 387–403, February 2011.

[5] Jiale, S., Jiao, Z., Song, G., and Kang, X., "Algorithm to identify the excitation inductance of power transformer with wye-delta connection," *IET Elect. Power Appl.*, Vol. 3, No. 1, pp. 1–7, January 2009.

[6] Rahimpour, E., Jabbari, M., and Tenbohlen, S., "Mathematical comparison methods to assess transfer functions of transformers to detect different types of mechanical faults," *IEEE Trans. Power Deliv.*, Vol. 25, No. 4, pp. 2544–2555, August 2010.

[7] Pourhossein, K., Gharehpetian, G. B., Rahimpour, E., and Araabi, B. N., "A vector-based approach to discriminate radial deformation and axial displacement of transformer winding and determine defect extent," *Elect. Power Compon. Syst.*, Vol. 40, No. 6, pp. 597–612, March 2012

[8] Ghanizadeh, A. J., and Gharehpetian, G. B., "Application of characteristic impedance and wavelet coherence technique to discriminate mechanical defects of transformer winding," *Elect. Power Compon. Syst.*, Vol. 41, No. 9, pp. 868–878, May 2013.

[9] Khrennikov, A. Y., "Fault detection of electrical equipment. diagnostic methods," *Automat. Control Eng. J.*, Vol. 2, No. 1, pp. 19–27, February 2013.

[10] Mokhtari, G., Hejazi, M. A., and Gharehpetian, G. B., "Simulation of on-line monitoring of transformer winding axial displacement using UWB waves," *XIX International Conference on Electrical Machines (ICEM 2010)*, Rome, Italy, 6–8, September 2010.

[11] Hejazi, M. S. A., Ebrahimi, J., Gharehpetian, G. B., Mohammadi, M., Faraji-Dana, R., and Moradi, G., "Application of ultra-wideband sensors for on-line monitoring of transformer winding radial deformations—a feasibility study," *IEEE Sensors J.*, Vol. 12, No. 6, pp. 1649–1659, June 2012.

[12] Golsorkhi, M. S., Hejazi, M. A., Gharepetian, G. B., and Dehmollaian, M., "A feasibility study on application of radar imaging for detection of transformer winding radial deformation," *IEEE Trans. Power Deliv.*, Vol. 27, No. 4, pp. 2113–2121, September 2012.

[13] Fear, E. C., Li, X., Hagness, S. C., and Stuchly, M. A., "Confocal microwave imaging for breast cancer detection: Localization of tumors in three dimensions," *IEEE Trans. Biomed. Eng.*, Vol. 49, No. 8, pp. 812–822, August 2002.

[14] Xie, Y., Guo, B., Xu, L., Li, J., and Stoica, P., "Multi-static adaptive microwave imaging for early breast cancer detection," *IEEE Trans. Biomed. Eng.*, Vol. 53, No. 8, pp. 285–289, August 2006.

[15] Klemm, M., Craddock, I. J., Leendertz, J. A., Preece, A., and Benjamin, R., "Radar-based breast cancer detection using a hemispherical antenna array—experimental results," *IEEE Trans. Antenna Propagat.*, Vol. 57, No. 6, pp. 1692–1704, June 2009.

[16] Li, X., and Hagness, S. C., "A confocal microwave imaging algorithm for breast cancer detection," *IEEE Microw. Wirel. Compon. Lett.*, Vol. 11, No. 3, pp. 130–132, March 2001.

[17] Guo, B., Wang, Y., Li, J., Stoica, P., and Wu, R., "Microwave imaging via adaptive beam-forming methods for breast cancer detection," *J. Electromagn.Waves Appl.*, Vol. 20, No. 1, pp. 53–63, 2006.

[18] Nilavalan, R., Gbedemah, A., Craddock, I. J., Li, X., and Hagness, S. C., "Numerical investigation of breast tumour detection using multi-static radar," *Inst. Elect. Eng. Electron. Lett.*, Vol. 39, pp. 1787–1789, December 2003.

[19] Craddock, I. J., Nilavalan, R., Leendertz, J., and Preece, A., "Experimental investigation of real aperture synthetically organised radar for breast cancer detection," *Proc. IEEE Antennas Propagat. Symp.*, Vol. 1B, pp. 179–182, July 2005.

[20] Aftanas, M., *Through Wall Imaging with UWB Radar Wystem*, Ph.D. Thesis, Technical University of Kosice, Slovakia, pp. 5–39, August 2009.

[21] Zhisong, W., Jian, L., and Renbiao, W., "Time-delay- and time-reversal based robust Capon beam-formers for ultra-sound imaging," *IEEE Trans. Med. Imag.*, Vol. 24, pp. 1308–1322, October 2005.

[22] Shao, W., Zhou, B., Zheng, Z., and Wang, G., "UWB microwave imaging for breast tumor detection in inhomogeneous tissue," *Proceedings of IEEE 27th Annual International Conference of the Eng. in Med. and Biol. Society (EMBS)*, pp. 1496–1499, Shanghai, 17–18 January 2006.

[23] Xu, L., Bond, E. J., Van Veen, B. D., and Hagness, S. C., "An overview of ultra-wideband microwave imaging via space-time beam-forming for early-stage breast-cancer detection," *IEEE Antennas Propagat. Mag.*, Vol. 47, No. 1, pp. 19–34, February 2005.

[24] Paul, M. K., Sagar, M. A. K., Hussain, S. U., and Rashid, A. B. M. H., "UWB microwave imaging via modified beamforming for early detection of breast cancer," *6th International Conference on Electrical and Computer Engineering (ICECE 2010)*, Dhaka, Bangladesh, 18–20 December 2010.

BIOGRAPHIES

Raziyeh Mosayebi received the B.S. and M.S. degrees in electrical engineering from Amirkabir University of Technology, Tehran, Iran, in 2011 and 2013, respectively. She is going to pursue Ph.D. studies in the signal processing field. During the B.S. and M.S. degrees, she worked at the Multimedia Signal Processing Research Lab at Amirkabir University. During this

period, she worked on digital signal processing with an emphasis on microphone arrays and multichannel signal processing. Her research interests include signal processing, multi-rate and subband signal processing, adaptive signal processing, microphone array processing, biomedical signal processing, blind source separation and source localization.

Hamid Sheikhzadeh received the B.S. and M.S. degrees in electrical engineering from Amirkabir University of Technology, Tehran, Iran, in 1986 and 1989, respectively, and the Ph.D. degree in electrical engineering from the University of Waterloo, Waterloo, ON, Canada, in 1994. He was a faculty member in the Electrical Engineering Department, Amirkabir University of Technology, until September 2000. From 2000 to 2008, he was a Principle Researcher with ON semiconductor, Waterloo, ON, Canada. During this period, he developed signal processing algorithms for ultra-low-power and implantable devices leading to many international patents. Currently, he is a faculty member in the Electrical Engineering Department of Amirkabir University of Technology. His research interests include signal processing, biomedical signal processing and speech processing, with particular emphasis on speech recognition, speech enhancement, auditory modeling, adaptive signal processing, subband-based approaches, and algorithms for low-power DSP and implantable devices.

Mohammad Sadegh Golsorkhi received his M.Sc. in electric power engineering from Amirkabir University of Technology Tehran, Iran in 2012, graduting as honored student. He is currently persuing his PhD degree in The University of Sydney, Sydney, Australia. His reasearch interests include renewable energy resources, microgrids and power transformers monitoring.

Maryam Sadat Akhavan Hejazi received the B.Sc. degree in electrical engineering in 2003 and the M.Sc. and Ph.D. degrees in electric power engineering from Amirkabir University of Technology, Tehran, Iran, in 2006 and 2011, respectively. Currently, she is Assistant Professor at the University of Kashan, Kashan, Iran. She is the author of more than 30 journal and conference papers. Her research interests include transformer monitoring and modeling, as well as distributed generation and smart grid.

Gevorg B. Gharehpetian received his BS, MS and Ph. D degrees in electrical engineering in 1987, 1989 and 1996 from Tabriz University, Tabriz, Iran and Amirkabir University of Technology (AUT), Tehran, Iran and Tehran University, Tehran, Iran, respectively, graduating all with First Class Honors. As a Ph. D student, he has received scholarship from DAAD (German Academic Exchange Service) from 1993 to 1996 and he was with High Voltage Institute of RWTH Aachen, Aachen, Germany.He has been holding the assistant professor position at AUT from 1997 to 2003, the position of Associate Professor from 2004 to 2007 and has been Professor since 2007. He is the author of more than 650 journal and conference papers. His teaching and research interests include Smart Grid, DGs, Monitoring of Power Transformers, FACTS Devices, HVDC Systems, and Power System Transients.